

# Particle removal in linear shear flow: model prediction and experimental validation

*M.L. Zoetewij<sup>\*</sup>, J.C.J. van der Donck and R. Versluis*

*TNO Science and Industry, P.O. Box 155, 2600 AD Delft, The Netherlands*

## **Abstract**

In many industrial processes, particle contamination is becoming a major issue. Particle detachment from surfaces can be detrimental, e.g. during lithographic processing. During cleaning however, detachment is aimed for. However, until recently, only little is known on the mechanism of particle detachment due to flowing gasses. In high throughput applications, large gas velocities are likely to occur at critical places in the system. It is possible to test particle behavior experimentally under all conditions that may arise. Therefore, the aim of this study is to be able to predict the risk of particle detachment by modeling.

For this purpose particle-surface interaction is studied for micron-sized particles. Based on the particle Reynolds number, critical particle diameters were determined for which the flow-induced forces on the particles (drag and lift forces) are larger than the attractive forces between the particle and the surface (Van der Waals force). Among the different

---

<sup>\*</sup> Corresponding author, electronic mail : [Marco.Zoetewij@tno.nl](mailto:Marco.Zoetewij@tno.nl) (M.L. Zoetewij)

possible particle motions (lift, sliding and rotation), particle rotation turns out to be the responsible mechanism of particle removal. A critical particle diameter was defined for which attracting and flow induced forces are equal. Calculated values of the critical particle diameter agree with the experimental results within several microns. This removal mechanism model can thus be used to calculate the cleaning efficiency of a flow, and for determining the probability of unwanted detachment of particles from the surfaces in an ultra clean production or processing environments.

## **1 Introduction**

For many industrial applications, a clean environment is essential to prevent processing errors. The particle exchange with the wall surface is a major concern.

In this article particle-surface interaction and the removal and transport of particles by gas flows at atmospheric conditions is studied in detail. Based on the particle and flow properties, the particle behavior can be predicted. The possible actions are categorized in

1. Complete removal by lift,
2. Sliding over the surface,
3. Rolling over the surface.

The relevant parameters and expressions are derived. In the current research, only the removal of solid particles with a flow of gas is investigated. The model was verified with experimental data.

## 2 Forces acting on the particles

Particles on a surface experience several forces. These forces can be related to the particle itself, or being induced by the flow field at the location of the particle. The relevant forces acting on a particle are shown schematically in Figure 1

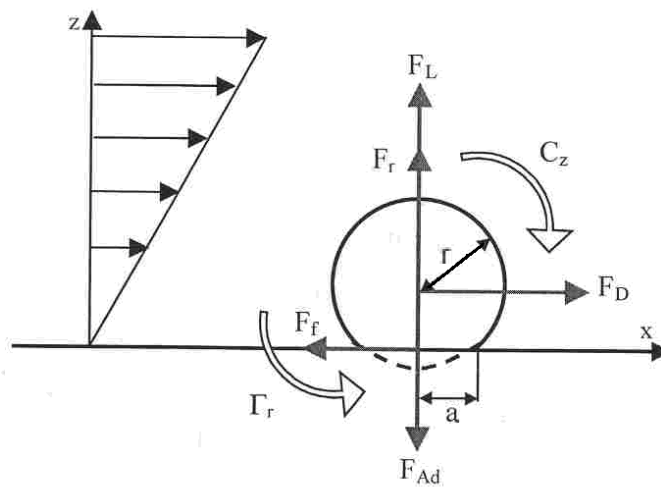


Figure 1 : Forces and torque acting on a particle in shear flow. Copied from [1].

### 2.1 Adhesive forces

The gravity force and the Van der Waals interaction are directly related to the particle, and not affected by the flow. Other attractive forces (e.g. electrostatic and capillary) are not included in the current model. The gravity force is given by

$$F_G = m \cdot g = \rho \cdot V \cdot g, \quad (1)$$

with  $m$  the particle mass and  $g$  the gravitational acceleration. The mass  $m$  equals density  $\rho$  times volume  $V$ .

The second contribution is the Van der Waals force, which is for a spherical particle given by

$$F_V = \frac{A_H \cdot d}{12z_0^2} \left( 1 + \frac{2a^2}{z_0 \cdot d} \right), \quad (2)$$

in which  $A_H$  is the material dependent Hamaker constant,  $d$  the particle diameter,  $z_0$  the particle-to-surface distance (usually assumed to be  $z_0=0.4$  nm) and  $a$  the contact area radius of the particle, as defined in Figure 2. The second term corrects for the contact area increase due to particle deformation. For a non-deformed spherical particle, the contact area is a point so  $a=0$  and the second term cancels.

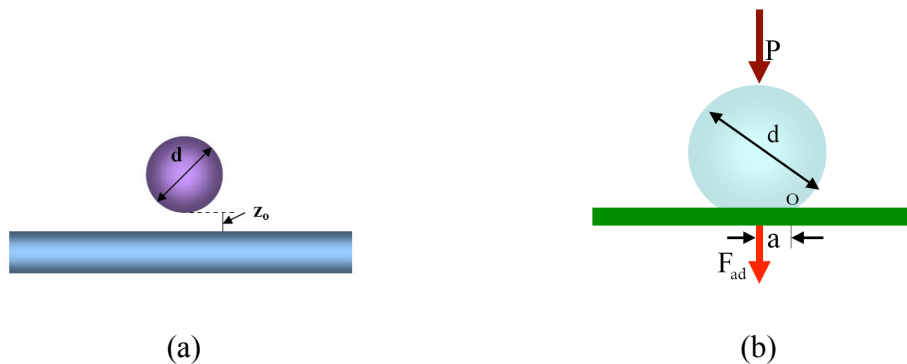


Figure 2 : Spherical particle of size  $d$  on a flat surface. The distance of nearest approach is defined by  $z_0$  (a). The contact radius  $a$  is defined by the deformation of the particle when an external load  $P$  is applied, shown in (b). Without external forcing,  $P=0$ , only the adhesive force  $F_{ad}$  is relevant. Figures from [2].

For simplicity, only spherical particles on flat surfaces are investigated, surface roughness of the particle or surface is not included. The plastic deformation of the

particle is implemented in the analysis. According to the JKR-theory, the contact radius of deformation can be calculated from the work of adhesion  $W_a$  of the particle [2]. Note that both the particle and the surface can deform, so properties of both materials, indicated by the subscripts 1 and 2 respectively, determine the contact radius  $a$  via the deformation constant  $K$ .

$$a = \sqrt[3]{\frac{3\pi \cdot W_a \cdot d^2}{2K}} \quad W_a = \frac{A_H}{12\pi \cdot z_0^2} \quad K = \frac{4}{3} \left[ \frac{1-\gamma_1^2}{E_1} + \frac{1-\gamma_2^2}{E_2} \right]^{-1}, \quad (3)$$

where  $E_{1,2}$  are the Young modulo and  $\gamma_{1,2}$  the Poisson ratios of both materials.

Based on the expressions for gravity and Van der Waals force, the two contributions can be compared. For most metals and glass particles, the gravity becomes important for particle diameters larger than 1.0 mm. For plastic materials, this transition occurs at 10 mm. For smaller particles, the gravity interaction (proportional to  $d^3$ ) can be neglected, and the Van der Waals force (proportional to  $d$ ) is the most relevant interaction. Electrostatic and capillary forces are not taken into account in the current analysis.

## 2.2 Removal forces

Any flow will exert forces on the particles, which can be classified in lift and drag forces. Near a no-slip surface, a boundary layer will be present in the flow. In this boundary layer, there is a gradient in the stream-wise velocity. Since close to the wall the velocities are small, a linear velocity profile is assumed in the boundary layer. The velocity gradient results in a lift force  $F_L$  acting perpendicular to the stream-wise direction, pointing towards the region with higher velocities. Since the particles are in the boundary layer of the fluid flow, these particle will experience a lift force  $F_L$  expressed by

$$F_L = 1.615 \cdot \eta \cdot d^2 \left( \frac{\rho}{\eta} \frac{\partial u}{\partial y} \right)^{1/2} U_p. \quad (4)$$

The  $(\partial u/\partial y)$  term denotes the gradient in y-direction of the velocity profile  $u(y)$ . The term must be evaluated at the centre of the particle, at  $y=d/2$ . The subscript p indicates that the flow velocity  $U_p$  at the particle location should be used to calculate the lift force. When the lift force is larger than the sum of the attracting forces, the particle will be lifted from the interface.

The drag force represents the force that is exerted on a body by a flow in stream-wise direction. The drag force is given by

$$F_D = \frac{1}{2} \rho U^2 \cdot C_D \cdot A, \quad (5)$$

with  $\rho$  the fluid viscosity,  $U$  the characteristic fluid velocity at the position of the body ( $=U_p$ ),  $C_D$  the drag coefficient and  $A$  the effective area of the particle perpendicular to the flow direction. The value of the drag coefficient  $C_D$  is for small particles (particle Reynolds number in the Stokes range  $10^{-4} < Re_p < 2$ ) given by

$$C_D = 1.7009 \cdot f = 1.7009 \frac{24}{Re_p}. \quad (6)$$

The term  $f=24/Re_p$  represents the friction on a spherical particle falling in a static fluid column [3]. The pre-factor 1.7009 corrects for the effect of the wall, which changes the flow pattern around the particle and thus the drag force [4].

The static friction of a body on a surface is expressed by the static friction factor  $\mu$ . The minimum force needed to overcome static friction is given by  $F_{friction} = \mu \sum F_{\perp}$ . The net

force perpendicular to the surface is given by the difference between attractive components (gravity and Van der Waals) and the lift force pointing in opposite direction. In situations where the drag force is larger than the static friction force, the particle will start sliding over the surface.

The third type of motion that the particle may experience as a result of flow interaction is rotation, which is related to the moment of surface stresses [5]

$$M_D = \frac{1}{2} \rho U^2 \cdot C_M \cdot V . \quad (7)$$

Here  $V$  is the volume of the particle and  $C_M$  a constant which equals

$$C_M = 0.943993 \cdot f = 0.94339 \frac{24}{\text{Re}_p} . \quad (8)$$

The factor 0.94399 corrects for the presence of the wall [4,6]. The expression  $f=24/\text{Re}_p$  is similar as used in the drag force calculations. Substitution of  $C_M$  in the equation of  $M_D$  results in

$$M_D = 0.943993 \cdot \eta \cdot 2\pi \cdot d^2 \cdot U_p . \quad (9)$$

### **2.3 Force and torque balance**

The motion of the particle is based on the force and torque balances between the relevant forces, as indicated schematically in Figure 1.

The particle will be elevated from the surface when the lift force is larger than the adhesive Van der Waals force and the gravity force  $F_L \geq F_V + F_G$ . When neglecting gravity (which is a valid assumption for sub-millimeter particles) and setting the lift force

larger or equal to the Van der Waals force, the critical particle diameter for lift can be calculated as

$$d_{lift} \geq \sqrt{\frac{A_H}{12z_0^2 \frac{1.615}{2} \sqrt{\rho\eta} \left(\frac{\partial u}{\partial y}\right)^{3/2}}} = \frac{(A_H)^{1/2}}{3.11 \cdot z_0} (\rho\eta)^{-1/4} \left(\frac{\partial u}{\partial y}\right)^{-3/4} = \zeta_{lift} \left(\frac{\partial u}{\partial y}\right)^{-3/4}. \quad (10)$$

The density  $\rho$  and viscosity  $\eta$  are fluid properties and the value  $(\partial u/\partial y)$  represents the local shear rate in the flow at the center of the particle.

For particle sliding, the inequality reads  $F_D \geq \mu_s (\vec{F}_V + \vec{F}_G + \vec{F}_L) = \mu_s (F_V + F_G - F_L)$  with the lift force acting oppositely to the other two contributions. For small particles, the gravity can again be neglected and the critical particle diameter for sliding can be calculated as

$$d_{sliding} \geq \frac{\mu_s \cdot A_H}{12z_0^2 \frac{1.7009 \cdot 3\pi}{2} \eta \frac{\partial u}{\partial y}} = \frac{\mu_s \cdot A_H}{96.2 \cdot z_0^2} \eta^{-1} \left(\frac{\partial u}{\partial y}\right)^{-1} = \zeta_{sliding} \left(\frac{\partial u}{\partial y}\right)^{-1}. \quad (11)$$

Particle rotation will occur when  $M_D + F_D L_1 + F_L L_2 \geq (F_V + F_G) L_2$ , with the values of  $L$  determined by the lengths of the arm of torque for the different forces.  $L_2$  equals the contact radius  $a$ . Assuming that the contact radius is very small compared to the particle diameter, the value of  $L_1$  can be approximated by the particle radius  $L_1 = d/2$ .  $M_D$  is the moment of the surface stresses. Since all terms have a different dependence on particle diameter  $d$ , a single expression cannot be derived for rotation.

### 3 Particle Reynolds number

The behavior of a fluid flow can be characterized by the dimensionless Reynolds number

$$Re = UL/\nu = UL\rho/\eta. \quad (12)$$

In a similar way, a particle Reynolds number  $Re_p = U_p d \rho / \eta$  can be defined which describes particle behavior in a flow. The particle diameter is indicated by  $d$ , and  $U_p$  indicates the characteristic stream-wise velocity at the location of the particle centre. The balances shown in the previous section can be related to the particle Reynolds number  $Re_p$ . For each motion, a critical particle Reynolds number can be defined based on the properties of the flow and the fluid [5]. The gravity and Van der Waals forces are combined and indicated by  $F_{attraction}$  in the expressions. When the particle Reynolds number is larger than one of the critical Reynolds numbers defined below, the particle will start moving accordingly.

$$Re_{lift} = \frac{F_{attraction}}{1.615d \sqrt{\frac{\rho}{\eta}} \sqrt{\frac{\partial u}{\partial y}}} \frac{\rho}{\eta^2}, \quad (13)$$

$$Re_{sliding} = \frac{\mu_s \cdot F_{attraction}}{1.7009 \cdot 3\pi + \mu_s \cdot 1.615 \cdot d \sqrt{\frac{\rho}{\eta}} \sqrt{\frac{\partial u}{\partial y}}} \frac{\rho}{\eta^2}, \quad (14)$$

$$Re_{rotation} = \frac{F_{attraction} \cdot L_2}{0.94399 \cdot 2\pi \cdot d + 1.7009 \cdot 3\pi \cdot L_1 + 1.615 \cdot d \sqrt{\frac{\rho}{\eta}} \sqrt{\frac{\partial u}{\partial y}} L_2} \frac{\rho}{\eta^2}. \quad (15)$$

Based on the particle Reynolds number and the different critical values, the motion of the particles can be predicted. In Figure 3, the results are shown for the situation of glass particles on a glass substrate, subjected to an air flow ( $p=1$  atm,  $T=293$  K) with a shear rate of  $2 \cdot 10^6 \text{ s}^{-1}$  at the interface.

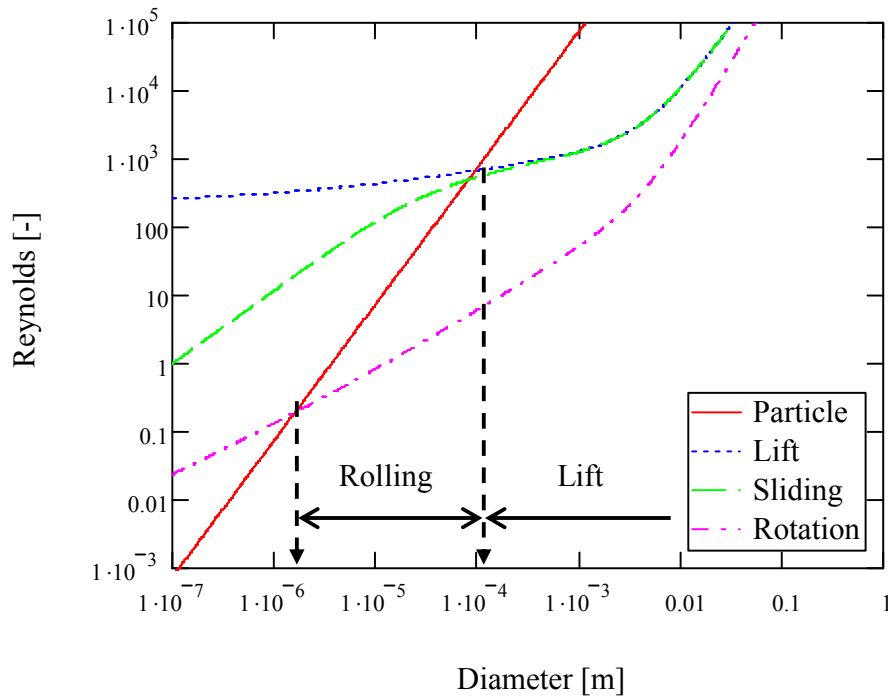


Figure 3 : Reynolds numbers in air flow with  $2 \cdot 10^6 \text{ s}^{-1}$  shear rate at the interface for glass particles on glass substrate. When the particle Reynolds number is larger than one of the other lines, the particle will start moving accordingly. Particles larger than  $1.6 \text{ }\mu\text{m}$  start rolling, and for diameters above  $100 \text{ }\mu\text{m}$ , particles are lifted. Particles smaller than  $1.6 \text{ }\mu\text{m}$  do not move.

The intersection points of the different Reynolds lines with the straight particle Reynolds number line indicate the critical particle diameter above which the corresponding motion becomes possible. Particle rotation becomes relevant at  $1.6 \text{ }\mu\text{m}$ , while particles larger than  $80 \text{ }\mu\text{m}$  will start sliding (and rotating). Complete lift occurs for particle diameters larger than  $100 \text{ }\mu\text{m}$ . Rotation is thus the most critical type of motion when dealing with micron sized particles. When a particle starts moving (rotating), the adhesive interaction

decreases since the distance between particle and surface increases. Another effect is that due to rotation particle does not have the flattened side connected to the surface any longer. The contact area decreases, and thus also the attraction between particle and surface.

For the situation of metal-metal and polystyrene-polystyrene, the graphs are shown in Figure 4. For the metal case, the critical diameters are close to those calculated for the glass particles. The polystyrene particles are much stronger attached to the surface, and flow interaction only becomes relevant for larger particle diameters, even when ignoring electrostatic interaction.

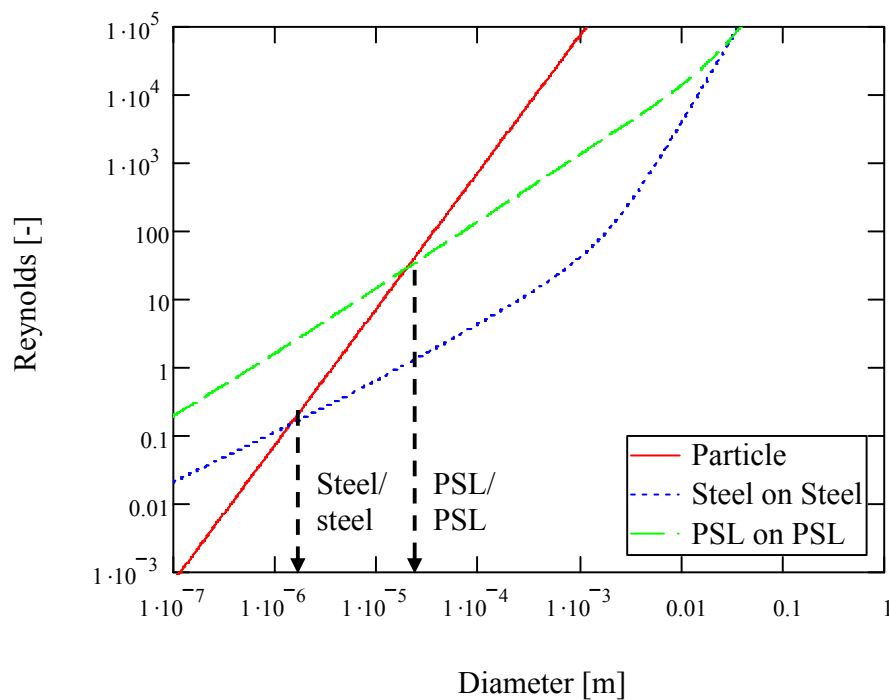


Figure 4 : The critical diameter for rotation for different materials. The situations for steel particles on a steel surface and PSL (polystyrene) on PSL are shown, both in air flow at  $2 \cdot 10^6 \text{ s}^{-1}$  shear rate.

Table 1 : Material properties (surface and particle same material). Shown are average values from various sources, as used in the calculations.

Property	Glass	Steel	Polystyrene	Units
Density	2500	8000	1100	$\text{kg/m}^3$
Hamaker constant	6.5	8.0	6.6	$10^{-20} \text{ J}$
Poisson ratio	0.29	0.3	0.29	-
Young's Modulus	8.0	20	0.31	$10^{10} \text{ Pa}$
Static friction coeff	1.0	0.75	0.50	-

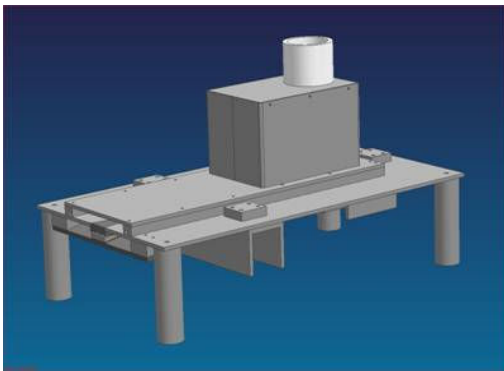
## 4 Experimental validation

The particle diameters calculated with the expressions derived in the previous chapter are validated with experimental data. These data are obtained from a flow-cell experiment, in which different wall shear rates can be obtained by changing the flow through the cell.

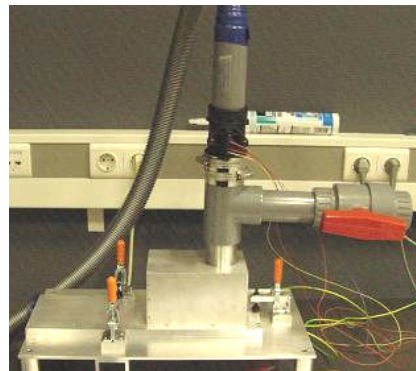
### 4.1 Experimental set-up

The set-up used for the experiments consists of a rectangular channel, as shown in Figure 5. The width of the channel is much larger than the height, which is only 10 mm. In this geometry, a well defined flow over the lower surface can be obtained. In the bottom plate, a stainless steel sample holder can be inserted. The metal housing and sample

holder are connected to grounded, so electrostatic forces are not relevant during the experiments. The flow is created using a pump which is connected to the upper side of the set-up (see Figure 5). During the experiment, the sample with particles is subjected to a uniform and constant air flow. The used particles are 5-10 micron sized crystals (Arizona Test Dust). The particles are distributed homogeneously over the sample holder prior to the experiments. The removal of particles took place within the first second of the flow. The duration of the flow in the experiments varied between 2 and 5 seconds at atmospheric pressure. Before and after the experiments, the number and positions of the particles were measured and counted.



(a)



(b)

Figure 5 : The left image shows the design of the flow-cell, on the right the actual set-up. The air flows in through the slit on the left side, and is removed with a pump at the top. The sample is inserted on the bottom of the slit for measurement.

#### 4.2 *Shear rates*

The turbulent velocity profile ( $Re > 10^4$ ) in the cell is calculated with CFD using the  $k-\epsilon$  model. The total mass flow measured in the experiments was used as an input parameter

for the simulations. At the wall, a no-slip condition was applied and no wall functions were used. In the wall region, the velocity profile was calculated to be linear with the distance to the wall (for distances below 0.1 mm in a 10 mm high channel). The shear rates obtained with the set-up range from  $7 \cdot 10^4$  up to  $2 \cdot 10^6 \text{ s}^{-1}$ . All particle diameters investigated in the experiments are well within the linear part of the velocity profile. The velocity gradient can thus for each individual experiment be taken constant in the Reynolds number calculations for the particle motion.

For the different shear rates, the residual percentage of particles on the sample was determined after being subjected to the flow. The particles were counted in 5 diameter classes, 0-5, 5-10, 10-20, 20-50 and 50-100  $\mu\text{m}$ . The residual percentages from the experiments are plotted at the centers of the diameter classes in figure 6. The total removal percentage obtained in the diameter range 20-50  $\mu\text{m}$  is plotted at  $d=35 \mu\text{m}$ .

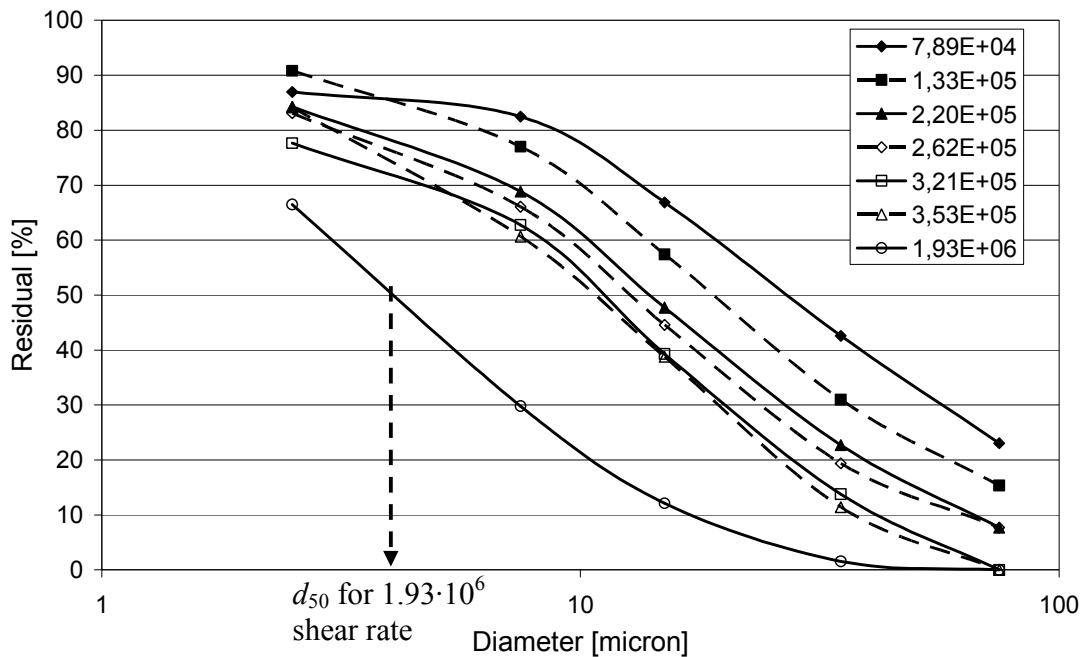


Figure 6 : The residual percentage versus particle diameter is shown. Apart from the curvature at both ends of the lines, a straight line can be fitted though the centre parts.

### 4.3 Characteristic particle diameter

From the graph shown in Figure 6, the  $d_{50}$  value is calculated, which is defined as the diameter for which 50% of the total amount is removed due to the flow (50% residual). For the shear rates corresponding to the experimental conditions, the critical diameters for lift, sliding and rotation are determined with the model. The critical diameter and the experimentally obtained  $d_{50}$  are shown in Table 2. The values  $d_{30}$  and  $d_{70}$  indicate the spread in the particle diameter distribution with  $d_{30}$  and  $d_{70}$  the diameters with 30% and 70% residual respectively.

Table 2 : Calculated ( $d_{\text{lift,slid,rot}}$ ) and measured ( $d_{50}$ ) diameters for different shear rates. The values  $d_{30}$  and  $d_{70}$  indicate the spread in the removal efficiency.

Shear [1/s]	$d_{\text{lift}}$ [ $\mu\text{m}$ ]	$d_{\text{rot}}$ [ $\mu\text{m}$ ]	$d_{50}$ [ $\mu\text{m}$ ]	$d_{30}\dots d_{70}$ [ $\mu\text{m}$ ]
$7.89 \cdot 10^4$	1740	25.6	27	58...13
$1.33 \cdot 10^5$	1047	16.3	19	36...10
$2.20 \cdot 10^5$	661	10.5	14	27...7
$2.62 \cdot 10^5$	566	9.1	12.6	25...7
$3.21 \cdot 10^5$	473	7.6	11.0	21...6
$3.53 \cdot 10^5$	436	7.0	10.5	20..6
$1.93 \cdot 10^6$	101	1.7	4.1	8..2

The diameters calculated for  $d_{\text{rot}}$  are close to the  $d_{50}$  values from the experiments. The difference is several microns at maximum. All values are under predicted ( $d_{\text{rot}} < d_{50}$ ) with a maximum deviation of 33 % (except for the last case with highest shear rate). The diameter values calculated for lift and sliding are about three orders of magnitude larger than the particles that moved in the experiments. Apparently, the removal in the experiment was due to rotation, and not to lift or particle sliding.

The diameters  $d_{\text{rot}}$  and  $d_{50}$  were determined for all individual cases of different shear rate. When plotting these diameters versus the corresponding shear rates, it shows power law behavior. Here also the systematic under prediction of  $d_{\text{rot}}$  compared to the experimental value for  $d_{50}$  is clearly visible. The behavior as predicted by the model is, with a small underestimation, also observed in the experimental data in Figure 7.

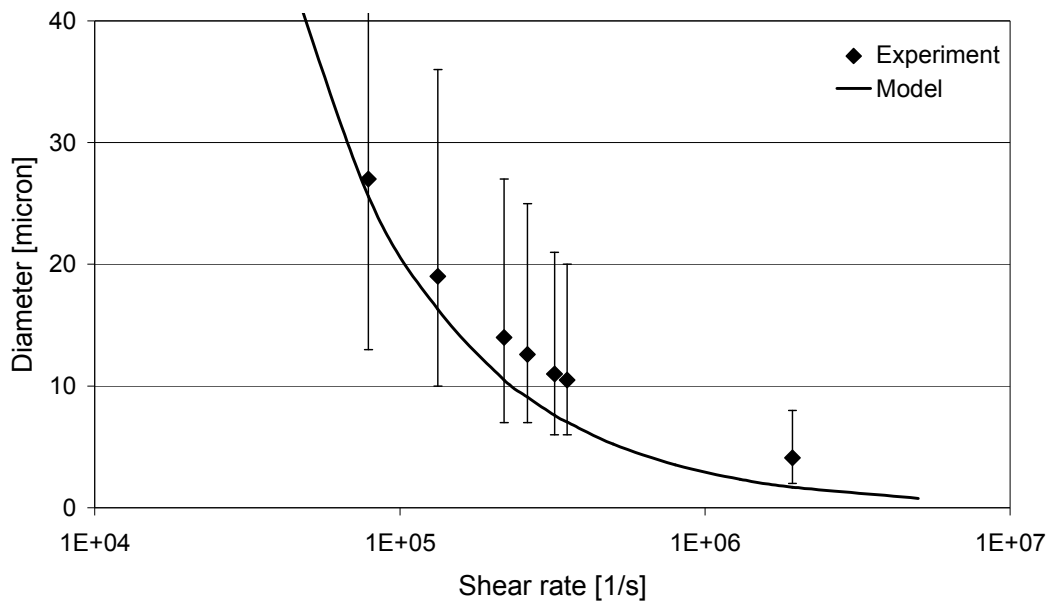


Figure 7 : Both the calculated critical diameter for particle rotation  $d_{rot}$  and the experimentally obtained diameter  $d_{50}$  (50% of the particles is removed) are shown for different shear rates. The model and the experimental data are in good agreement. The model prediction is on average 3 micron below the experimentally observed diameter, which makes the model a safe estimate for particle movement probability. The points of the experimental data indicate the diameter from which 50% of the particles is removed. The error bars indicate the 30% and 70% removal diameters.

The experimental data shows reasonable agreement with the particle rotation model, although the choice of 50% removal is rather arbitrary. The model only calculates the static force and torque balance on an isolated particle. Because in the experiments, the dynamic process is measured, this also involves a probability distribution for the removal.

Since there are many particles, the flow will also be affected by the presence of other particles. The systematic underprediction could be a consequence of surface roughness which is not included in the model. In reality, particles can have irregular shapes, instead of the assumed spherical geometry. These particles can have a larger contact area and a smaller area of fluid impact. All these effects result in a higher attractive interaction, which would result in a larger critical diameter when taking these effects into account.

## **5 Discussion**

The model is based on a fixed value for the adhesive Van der Waals force. In reality, there is a distribution in adhesion energy between particle and surface, and thus also in attraction force. Due to surface roughness, the particle to surface distance becomes slightly larger, which implies a lower attraction force. When a small particle fits into the roughness of the surface, the attraction will be higher than expected. For non-spherical particles, the attraction will be higher than calculated based on diameter when the particle is aligned with the surface. The average value of  $d_{50}$  is a good measure for the diameter corresponding to the average interaction force.

The removal of the particles in the experiments matched the diameter for the rotation mechanism; the diameters calculated for lift and sliding are much larger than the particle diameters that were removed. For spherical particles on a flat surface, the particles start rotating quite easily. For surfaces with roughness, the obstacle or barrier height determines the point of rotation. The surface roughness makes rotation more difficult, and hence larger critical particle diameters will be obtained.

For small size particles, the diameter is underestimated by several microns. Since only Van der Waals interaction is included for the adhesion, there is a systematical difference between experimental results and the model predictions. The model assumes no surface roughness, while in reality the surface of the substrate and the particles are not perfectly smooth. Small particles tend to settle in the surface imperfections, where the attractive force is higher. Another effect is the electrostatic interaction, which may probably not be neglected for particles in the micrometer range. The Van der Waals and electrostatic forces are of the same order of magnitude for these particle sizes.

## **6 Conclusions**

Under the assumption of spherical solid particles on a flat surface, the interaction with a flow of air is investigated. Based on the balance of the various relevant forces, it is evaluated when and how a particle will start moving. The movement is classified in three regimes for lift, sliding and rotation. For small particles, with diameter in the order of 1 micron, the particles start rotating when the flow induced torque is larger than the torque of the Van der Waals force. When a particle starts rotating, the forces change, and complete removal becomes feasible. The experimental results show particle diameter for removal that compare within several micron with the rotational diameter calculated with the model. The diameters predicted by the model are slightly lower than observed in the experiments, which makes the model a conservative estimator of particle detachment. Since all particles are different of shape and orientation, the calculated values indicate an average particle diameter. Also some of the smaller particles will be removed, while

some larger particles will remain at the surface when subjected to a flow. The distribution in the diameter is quite large. Particles with the average diameter will be removed for 50%, particles of half of the average diameter by 30% and double the average diameter by 70%. The systematic underprediction of this diameter could be due to the fact that surface roughness, particle shape and electrostatic forces are neglected in the model. Especially for small size particles, these effects become more important.

## **Acknowledgements**

The authors want to thank Ruud Schmits and Wim Peterse for performing the experiments, Arnout Klinkenberg for the CFD calculations on the flow distribution in and Anton Duisterwinkel for the useful discussions. A part of the work is financially supported by VSR (Association for Cleaning Research).

## **References**

- 1 P. Schmitz, J. Cardot; Adhesion and removal of particles from charged surfaces under a humidity-controlled air stream, In "Particles on surfaces 7: Detection, adhesion and removal" (2002), Ed. K.L. Mittal, VSP, Utrecht, 189-196.
- 2 G. Ahmadi, Lecture notes course ME437/537. Clarkson University
- 3 W Chen, J. Sedimentary Research 73, 714 (2003).
- 4 A.J. Goldman, R.G. Cox, and H. Brenner, Chem. Eng. Sci. 22, 653 (1967).
- 5 Y Mamono, K. Yokogawa, and M. Izawa, J. Vac. Sci. Tech. B 22, 268 (2004).
- 6 G.M. Burdick, N.S. Berman, and S.P. Beaudoin, J. Nanoparticle Research 3, 455 (2001).